ACS OMEGA

Open Access

http://pubs.acs.org/journal/acsodf

Article

Antimicrobial and Virus Adsorption Properties of Y-Zeolite Exchanged with Silver and Zinc Cations

Perla Sánchez-López, Kevin A. Hernández-Hernández, Sergio Fuentes Moyado, Rubén D. Cadena Nava, and Elena Smolentseva*

Cite This: *ACS Omega* 2024, 9, 7554−7563

Read Online

ACCESS | Metrics & More | Article Recommendations

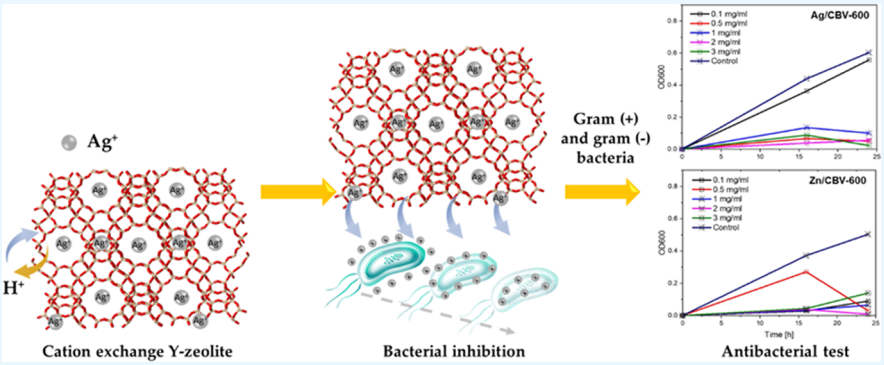

ABSTRACT: The antimicrobial activity of silver and zinc exchanged cations in Y-zeolite (Ag/CBV-600, Zn/CBV-600) is evaluated against *Staphylococcus aureus* (gram (+)) and *Escherichia coli* (gram (−)) bacteria along with their adsorption capacity for viruses: brome mosaic virus (BMV), cowpea chlorotic mottle virus (CCMV), and the bacteriophage MS2. The physicochemical properties of synthesized nanomaterials are characterized by inductively coupled plasma optical emission spectroscopy (ICP-OES), UV−Vis spectroscopy, X-ray diffraction (XRD), and scanning electron microscopy (SEM). According to the obtained results, the main species associated with the exchanged ions are Ag^{+} and Zn^{2+} cations with the concentration of around 1 atomic %. The incorporation of cations does not modify the Y-zeolite framework. The Ag/CBV-600 and Zn/CBV-600 materials show an inactivation of 90% for both gram (+) and gram (−) bacteria at 16 h at a relatively low concentration of nanomaterial (0.5 mg/mL). Moreover, the samples present good adsorption capacity for BMV, CCMV, and MS2 viruses showing adsorption higher than 40% after 2 h of interaction with the viruses. These prominent results allow the further usage of nanomaterials as an effective remedy to inhibit and reduce the spread of viruses such as SARS-CoV-2 or other gram (+) or gram (−) bacteria.

1. INTRODUCTION

During the past few years, the development of nanotechnology has played a crucial role in the design, synthesis, and application of different types of nanomaterials. Nowadays, metal nanoparticles (NPs) are widely used for healthcare, agriculture, ecology, energy, and catalysis due to their unique optoelectronic, physicochemical, antimicrobial, and catalytic properties.[1−3] A wide variety of nanoparticles are explored for numerous biomedical applications, such as disease prevention and diagnostics, as well as in improving delivery systems of antiviral agents.[4,5] In this context, nanotechnology works and will continue to do so as a bridge for the development of nanomaterials with medical applications.[6]

It is well known that silver has antibacterial properties *per se*.[7,8] For many centuries, silver was used as an antimicrobial agent to prevent the spread of infections. There is a lot of literature devoted to the antibacterial applications of silver cations and nanoparticles.[9−13] The mechanism that manifests silver nanoparticles against bacteria may be explained as follows. Nanoparticles continuously release ions that migrate to the bacterial cell membrane and bind with the proteins. Due to their electrostatic attraction and affinity for sulfur proteins, metal ions can attach to the cell wall and cytoplasmic membrane. The attached ions increase the permeability of the cytoplasmic membrane and cause their rupture. Otherwise, in the case that the cells consume the metal ions, respiratory enzymes are deactivated and generate reactive oxygen species, which interrupt the production of adenosine triphosphate, the

Received: August 29, 2023
Revised: October 27, 2023
Accepted: November 2, 2023
Published: February 7, 2024

main nucleotide for cellular energy. Since sulfur and phosphorus are the key components of deoxyribonucleic acid (DNA), the interaction of ions with them may cause problems of DNA replication and cell reproduction or even lead to the death of microorganisms.[8,14]

Ag NPs demonstrate potent biocidal effects for some microorganisms such as *Staphylococcus aureus* (*S. aureus*), *Escherichia coli* (*E. coli*), *Pseudomonas aeruginosa* (*P. aeruginosa*), and *Candida albicans* (*C. albicans*), commonly used for antimicrobial tests. Such biosynthesized Ag NPs exhibit antimicrobial activity against model bacteria, *E. coli*, as reported by Maiti. [10]. Ag NPs synthesized via whole plant extract of Carduus crispus showed antibacterial activity on both the gram (−) bacterium *E. coli* and gram (+) bacterium *Micrococcus luteus*.[15] Green-synthesized Ag NPs (4.06 nm) using pu-erh tea leaf extract were evaluated against *E. coli*, *Klebsiella pneumoniae*, *Salmonella typhimurium*, and *Salmonella enteritidis*. Results demonstrate significant antibacterial activity against the selected gram (−) foodborne pathogens.[16]

Recently, it was found that zinc oxide may also be used in different areas to control antimicrobial activity.[17] For example, it can be used to combat a variety of microorganisms, such as *S. aureus*,[18−20] *E. coli*[14], and *C. albicans*.[21,22] Furthermore, ZnO has greater advantages due to its highest photocatalytic activity. In addition, ZnO exhibits good selectivity and better durability and heat resistance.

Many scientific reports are devoted to the synthesis of colloidal, supported, and immobilized nanoparticles using physical, chemical, and biological approaches.[23−27] Frequently, Ag and Zn ions are exchanged with the Na cations originally present in the zeolite that permits their uniform distribution in the pores of the zeolite matrix. The usage of zeolites helps to reduce the metal concentration, obtain stable particles in the nanometer range, and anchor nanoparticles into the channels and cavities of the support, avoiding their migration, agglomeration, and removal. Moreover, zeolites are characterized by a well-defined structure, reversible binding of small molecules, shape and size selectivity, and the ability to behave like metalloenzymes that regulate the immune system.[28,29] Also, zeolites are considered biocompatible and nontoxic materials. For example, clinoptilolite (natural zeolite) is used as a food additive providing essential minerals for individuals and may be used as an adsorbent of harmful substances that contaminate the environment, air, water, and food. Zeolites are characterized by antimicrobial properties *per se* and may also be combined with nanoparticles, increasing their antimicrobial effect.[30,31] It was shown that composite materials containing clinoptilolite manifest antibacterial activity toward *E. coli* and *S. aureus* strains.[32] However, the most common way to increase the antimicrobial activity of zeolites is combining them with Ag or Zn ions.[29,33] For example, silver-embedded zeolite A exhibits antibacterial properties against *E. coli*, *Bacillus subtilis*, and *S. aureus*.[34] Furthermore, X-type zeolite impregnated with silver demonstrates a bactericidal effect against *E. coli*, *S. aureus*, and *P. aeruginosa*.[35] The antimicrobial properties of silver cations exchanged into faujasite are studied.[36] High activity is shown for the majority of tested bacterial and fungal strains: *E. coli*, *Serratia marcescens*, *B. subtilis*, *Bacillus megaterium*, *Trichoderma viride*, *Chaetomium globosum*, *Aspergillus niger*, and *Cladosporium cladosporioides*. The material inhibits the growth of the tested microorganisms by 90−95%.[35]

Zn^{2+}- and Cu^{2+}-exchanged X-zeolite samples are studied against *E. coli*, *S. aureus*, and *P. aeruginosa*; also, their antifungal activities are tested against *C. albicans* and *Aspergillus niger* by the disc diffusion method.[37] Bimetallic materials Ag−Zn and Ag−Cu based on the NaY zeolite evaluated in vitro demonstrate antimicrobial potential against bacteria *E. coli* and the yeast *Saccharomyces cerevisiae* as a strain indicator. All materials showed good antimicrobial properties with the pair Zn−Ag being the most active among the tested bimetallic materials.[38]

The aim of this work was to find an alternative to antimicrobial materials based on nanoparticles, which would contain active silver and zinc immobilized into a solid matrix that prevents their agglomeration and migration to the environment. In the present work, silver and zinc ions exchanged with Y-zeolite (CBV-600) were microbiologically analyzed against strains of the bacteria *Staphylococcus aureus* and *Escherichia coli*; also, the physicochemical properties of the synthesized nanomaterials were determined. Finally, the adsorption results of different virus models such as the brome mosaic virus (BMV), cowpea chlorotic mottle virus (CCMV), and the bacteriophage MS2 were evaluated. Prominent results were obtained that may be helpful for the further understanding of the inhibition mechanism of pathogens using nanomaterials and prevent the spread of viruses such as SARS-CoV-2 or other gram (+) or gram (−) bacteria.

2. EXPERIMENTAL SECTION

2.1. Ion Exchange of Ag and Zn Cations. Y-zeolite with an atomic ratio of Si/Al = 2.6 and hydrogen nominal cation form was supplied by Zeolyst International (Product CBV-600, Zeolyst Int., Conshohocken, PA, USA). Ag^+ and Zn^{2+} cations were exchanged with hydrogen cations of the Y-zeolite using precursor solutions of $AgNO_3$ and $Zn(NO_3)_2$ (Sigma-Aldrich products) prepared at 0.1 N concentration under pH 4.2 ± 0.1 and 5.6 ± 0.1 for silver and zinc, respectively. The ion exchange method was applied at room temperature for 24 h under constant stirring with a ratio of 1 g of CBV-600 per 52 ± 2 mL of the precursor solution as reported in ref 39. After the ion exchange procedure, the samples were filtered, washed with deionized water, and dried at 110 °C for 20 h. Dried samples were stored in a plastic vial at room temperature, avoiding direct contact with UV radiation. Sample labels present the cations incorporated during the ion exchange following the zeolite product code: Ag/CBV-600 and Zn/CBV-600.

2.2. Material Characterization. The metal concentration in the prepared samples was determined by inductively coupled plasma optical emission spectrometry (ICP-OES Varian Vista-MPX CCD simultaneous) and compared to the standard calibration curve prepared with Ag, Al, Si, and Zn. Typically, 15 mg of the solid sample was dissolved in 43 mL of the acid mixture (HF, HNO_3, H_3BO_3). After that, samples were diluted with water and analyzed. Measurements were carried out in triplicate, and blanks were characterized using the same procedure.

The crystalline structure of the CBV-600 zeolite, before and after the metal exchange, was determined by powder X-ray diffraction (XRD) in a Panalytical AERIS diffractometer using Cu Kα (λ = 1.54184 Å) radiation. The interval of XRD analysis was 5−55° 2θ, with a step size of 0.02° and 1 s measuring time for each step.

The electronic transitions of the samples were studied by diffuse reflectance UV−visible spectroscopy (DRS) using a Cary 100 spectrophotometer (Agilent Technologies Mexico,)

https://doi.org/10.1021/acsomega.3c06462
ACS Omega 2024, 9, 7554−7563

in the wavelength range of 200−800 nm, with a resolution of 0.1 nm. The spectrum of CBV-600 was subtracted from the spectra of M/CBV-600 samples.

A Hitachi model H-7500 transmission electron microscope (TEM) was used at different magnifications to determine the size distribution of the virus particles and the formation of expected mesopores. 6 μL of sample was placed on solid support copper/400 mesh carbon grids (TedPella) and held on the grid for 90 s. Once this time passed, the excess sample was removed with Whatman No. 2 filter paper. If a contrast agent was required, 6 μL of 4% uranyl acetate was added to the grids and left to rest for 90 s before removing the excess. The samples mounted on their respective grids were stored in a desiccator for later transfer to the microscope. To calculate the virus diameter, micrographs were analyzed using scientific image manipulation software DigitalMicrograph. The hydrodynamic radius of the synthesized nanomaterials was determined by dynamic light scattering (DLS) on a Zetasizer Nano ZS from Malvern. 100 μL of sample was placed in a ZEN0040 polystyrene microcell to carry out three series of measurements in order to obtain a graph distribution of the hydrodynamic radius for the analyzed particles. In turn, an analysis of the zeta potential of the particles was carried out using DTS1070 cells. The obtained zeta potential values allowed determining the stability of the synthesized NPs and their tendency to avoid agglomerate formation.

2.3. Antibacterial Activity of Y-Zeolite in LB Medium. A colony of *E. coli* or *S. aureus*, cultivated on a lysogeny broth (LB)-agar plate, was added to 20 mL of LB medium and left shaking in an incubator (New Brunswick Scientific G-25) at 37 °C overnight. From the culture, 900 μL was taken and added to 45 mL of LB medium. The sample was incubated under shaking for 1 h, at 37 °C, until it reached 0.1 optical density at 600 nm (OD600). Then, different concentrations of Y-zeolite (0.1, 0.5, 1, 2, and 3 mg/mL) were added into 1.5 mL microcentrifuge tubes that contain the bacterial cultures, and each sample was triplicate. Two controls were included: LB medium with the zeolite and without bacteria and that with bacteria and without the zeolite. The microcentrifuge tubes were shaken at 37 °C in the incubator horizontally to allow good dispersion of the nanomaterial that is not soluble in the water. The OD600 measurements of bacterial growth were taken at 16 and 24 h in a 96-well plate (Corning Costar plates) on a UV−Vis spectrophotometer (Thermo Scientific Multiskan GO).

2.4. Bacterial Susceptibility Tests. 50 μL of fresh cell culture of *E. coli* or *S. aureus* with an OD600 equal to 0.1 was put on a LB-agar Petri dish plate (9 cm). Then, sterile filter paper discs of 0.5 cm in diameter were added to the plate. After that, 4 μL of the solution of a zeolite was applied onto each paper disc. Ampicillin was used as a positive control. Subsequently, the Petri dishes containing the samples were incubated for 16 h at 37 °C and then analyzed.

2.5. Production and Purification of CCMV and BMV Virus. The production of bromine mosaic virus (BMV) and cowpea chlorotic mottle virus (CCMV) was carried out under the protocol described by Cadena-Nava et al.[40] After 2 weeks of seed germination, the initial leaves were mechanically inoculated. The inoculation was done by delicately rubbing and scraping the upper leaf surfaces with a steel wool fiber, and 20 μL of virus (0.1 μg/μL) solution was applied to each leaf. At two weeks following the virus inoculation, the leaves exhibited characteristic signs of infection, specifically chlorosis in the form of spot or line patterns on leaves infected, respectively, by the CCMV and BMV. The leaves were blended with a virus extraction buffer (0.5 M sodium acetate, 0.08 M magnesium acetate, pH 4.5, 1% (v/v) β-mercaptoethanol). After blending, the leaf solution was filtered through cheesecloth, and then, a quarter of the volume of chloroform was added while stirring. Subsequently, the solution was centrifugated at 8,000 rpm using a JA-14 rotor for 40 min, at 4 °C within a Beckman Avanti JXN-26 centrifuge. The supernatant was collected and centrifuged again. The resulting pellet was discarded, and the solution was subjected to continuous agitation for at least 2 h at 4 °C to evaporate the excess of chloroform. Virus precipitation was done with 10% PEG8000 under stirring overnight, followed by centrifugation for 30 min at 4 °C. The resulting pellet was resuspended in 20 mL of virus suspension buffer (50 mM sodium acetate, 8 mM magnesium acetate, pH 4.5). Finally, the purified virus was obtained by 10% sucrose cushion ultracentrifugation at 32,000 rpm for 2 h, at 4 °C using an AW32Ti rotor of a Beckman XPN100 ultracentrifuge. The virus pellet was resuspended in virus buffer and stored at −80 °C.

2.6. Production and Purification of the MS2 Virus. A preinoculum of *E. coli* C-3000 was prepared in LB medium containing ampicillin (100 μg/mL). For the preinoculum, 100 μL of *E. coli* C-3000 was added to 5 mL of LB−ampicillin medium and incubated overnight at 37 °C under shaking at 250 rpm. Then, 200 μL of preinoculum was added to 5 mL of LB−ampicillin medium and incubated at 37 °C under shaking until the OD600 reached 0.5−0.7. After that, 5 mL of culture was added to 45 mL of LB medium with ampicillin and it was incubated at 37 °C, until the OD600 was in the range of 0.3−0.5. Then, 108 plaque-forming units (pfu) of bacteriophage MS2 was added to the last host cell culture. The culture was incubated overnight at 37 °C and shook at 250 rpm. On the next day, the culture was centrifuged at 8000 rpm for 50 min and the supernatant was collected. To purify the MS2 virus from the supernatant, the same methodology was utilized as that for the purification of the BMV and CCMV. For MS2 purification, the virus buffer was replaced by the TNE buffer (50 mM Tris-base, 100 mM NaCl, 5 Mm EDTA, pH 7.5).

2.7. Adsorption of Viruses with Nanomaterials. To evaluate the ability of materials to trap viruses, 0.5 mg of the corresponding nanomaterial was placed in a microcentrifuge tube and 0.05 mg of virus was subsequently added. The sample of the nanomaterial with the virus was brought up to a volume of 500 μL and gently mixed. Then, the sample was incubated at 5, 15, 30, 60, and 120 min at room temperature in a Mini Lab Roller. Afterward, each sample was centrifuged at 12,000 rpm for 5 min at 4 °C; the pelleted material was discarded. Later, the absorbance of the supernatant was measured at a wavelength of 260 nm to quantify the virus in the solution. The assays were performed in triplicate.

3. RESULTS AND DISCUSSION

3.1. Chemical Composition. The chemical compositions of the nanomaterials are presented in Table 1. The Si/Al atomic ratio for Y-zeolite experimentally obtained was 2.67, which is extremely close to the data provided by the supplier. After ion exchange, the Si/Al atomic ratio remained stable (Table 1), confirming that the ion exchange treatment did not produce any changes in the chemical composition of the zeolite structure, such as dealumination or disilation. The

https://doi.org/10.1021/acsomega.3c06462
ACS Omega 2024, 9, 7554−7563

Table 1. Elemental Composition of the Samples Measured by ICP-OES

	metal loading, (atomic percentage, %)				
sample	Si	Al	Ag	Zn	Si/Al
CBV-600	38.2	14.2			2.67
Ag/CBV-600	35.3	12.7	1.0		2.7
Zn/CBV-600	42.6	15.4		0.9	2.7

atomic concentrations of silver and zinc after ion exchange were practically the same (~1 at %).

3.2. X-ray Diffraction. The X-ray diffraction patterns of the Y-zeolite before and after ion exchange with Ag^+ and Zn^{2+} cations are shown in Figure 1. The obtained materials

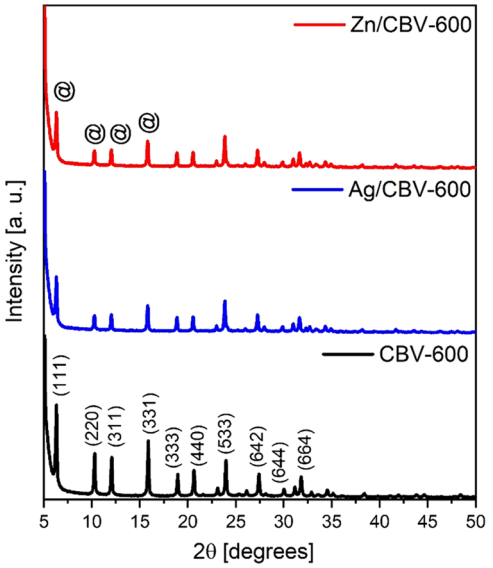

Figure 1. XRD patterns of the CBV-600 zeolite before and after ion exchange with Ag and Zn.

exhibited the typical pattern of the parent HY zeolite. Diffractograms revealed that the characteristic peaks of Y-zeolite remained at the same positions of the 2Θ angular interval after ion exchange with the metals. However, the variations of the relative intensities of several peaks were sensitive to Ag^+ and Zn^{2+} incorporation, in particular the planes (111) at 6.3°, (220) at 10.3°, (311) at 12.1°, and (331) at 15.9° labeled with "@" (see Figure 1). As reported previously,[41] the relative intensity changes in the diffraction peaks of zeolite after the ion exchange process, especially with transition metals, are mainly associated with the changes in the local structure (exchange sites) of the zeolite. The latter allowed us to conclude the preferential location of the different metal cations. Also, the variation in the intensity is strongly influenced by the metal charge on the support.[41] Despite the light changes in the local structure, it may be concluded that the zeolite structure remains stable after ion exchange with Ag^+ and Zn^{2+} cations because neither additional peaks nor any shift of characteristic signals was observed in the diffractograms. Therefore, the absence of silver and zinc phases may be attributed to their ionic noncrystalline form, which also was confirmed by UV−visible spectroscopy. Thus, the cationic species and small metallic clusters of silver and zinc were finely incorporated into the Y-zeolite exchangeable sites.

3.3. UV−Visible Spectroscopy. UV−visible diffuse reflectance spectra of the samples are shown in Figure 2. The UV−visible spectrum for CBV-600 reference samples (Figure 2(a)) was characterized by relatively small light absorption at 200−350 nm due to the structural imperfection of the zeolite crystals. The main contribution of the ionic species for exchanged metals was clearly observed after the subtraction of UV−visible spectra corresponding to CBV-600 from the UV−visible spectra for Ag/CBV-600 and Zn/CBV-600.

The spectrum of Ag/CBV-600 showed three characteristic bands at 213, 285, and 340 nm associated with Ag^+ ions and ionic and metallic clusters (Figure 2(b)). Generally, the bands between 200 and 300 nm are attributed to isolated Ag^+, $Ag_n^{\delta+}$, and Ag_m clusters in the zeolite structure.[42−45] The absorption band at 213 nm was linked with the charge transfer of Ag^+ ions ($[Kr]4d^{10}$-$[Kr]4d^9 5s^1$), which replaced the H^+ ions in the zeolite framework.[46−48] Two absorption bands at 285 and 340 nm with low intensity were related to ionic ($Ag_m^{\delta+}$, $3 < m < 7$) and metallic (Ag_m, $m \geq 8$) clusters with a limited number of atoms, respectively.[49−52] Similar results are reported in ref 53 for silver exchanged with natural zeolite (clinoptilolite and barrerite) showing silver ions and cluster species mainly.

A weak absorption band between 200 and 550 nm (centered at ca. 350 nm) was observed for the Zn/CBV-600 sample (Figure 2(c)). According to the literature data, zinc supported on zeolites has an absorption peak around 370 nm that is associated with ZnO, when the metal loading is higher than 1

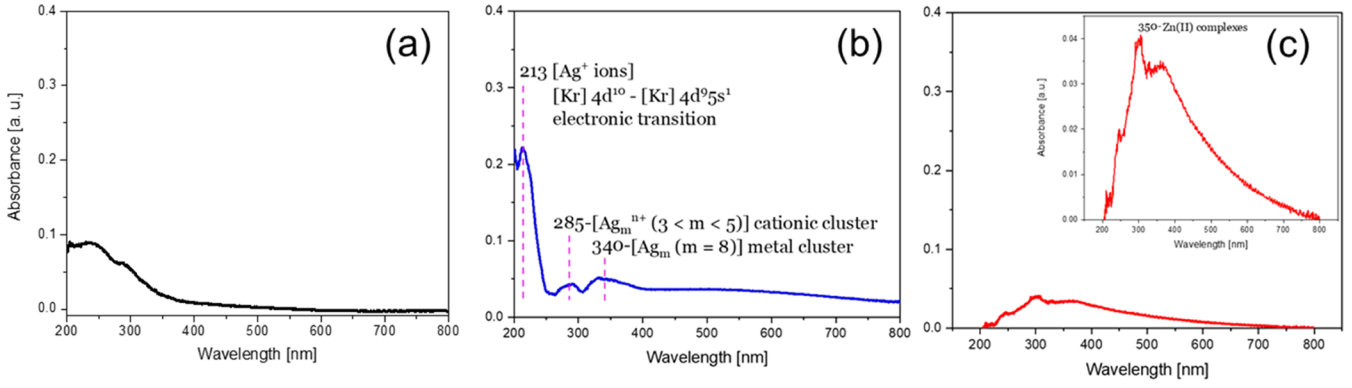

Figure 2. UV−visible spectra of (a) CBV-600 as a reference sample and spectra after ion exchange with cations: (b) Ag and (c) Zn. The spectra of samples after ion exchange are presented with subtraction of the CBV-600 spectrum.

https://doi.org/10.1021/acsomega.3c06462
ACS Omega 2024, 9, 7554−7563

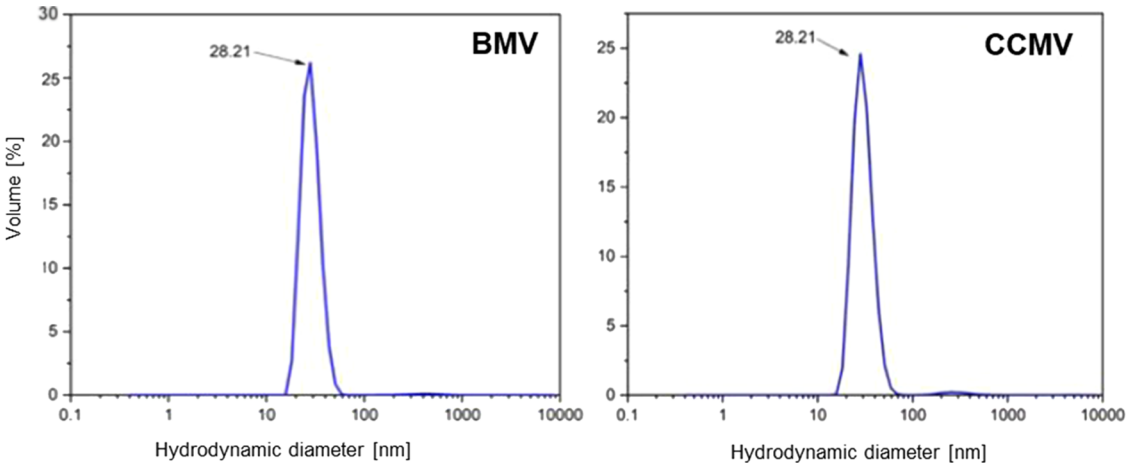

Figure 3. Hydrodynamic diameter for BMV and CCMV obtained using the DLS technique.

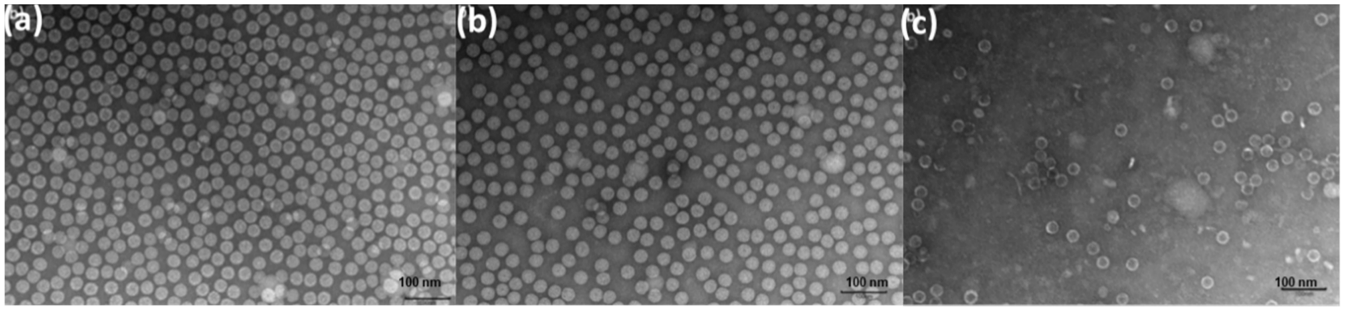

Figure 4. Transmission electron micrographs of BMV particles (a), CCMV particles (b), and MS2 particles (c). The scale bar is 100 nm.

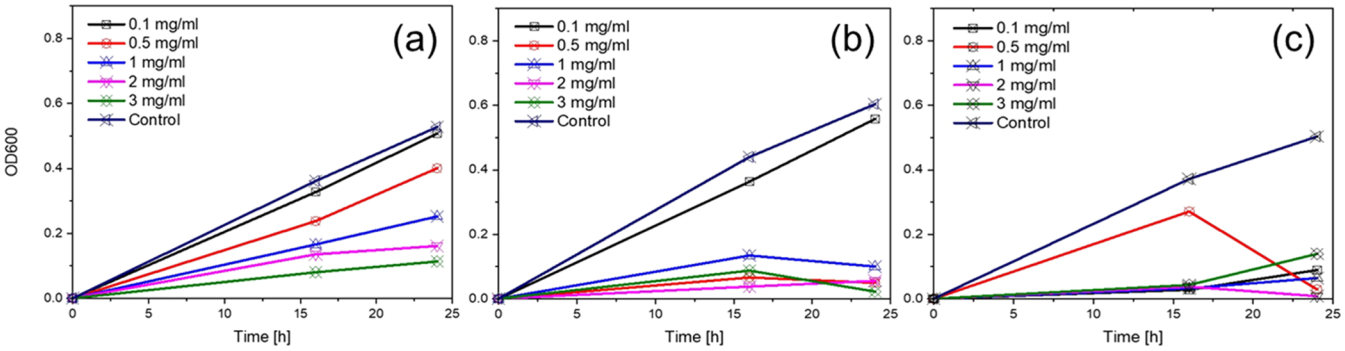

Figure 5. Antimicrobial activity of studied materials against *Escherichia coli* in terms of optic density at 16 and 24 h: (a) Y-zeolite, (b) Ag/CBV-600, and (c) Zn/CBV-600.

wt % and the absorption bands at 265−280 nm correspond to ZnO clusters.[54,55]

The faujasite structure has several positions, where the exchanged cations may be located in order to compensate the negative charge of the lattice: the hexagonal prisms (site I), the sodalite cages (site I′ and II′), or the supercages (sites II, III, and III′) of the framework.[56,57] The ionic radius of silver is 1.14 Å, which implies that silver species preferentially occupied sodalite cages and supercages. However, zinc characterized by 0.74 Å ionic radius may be located in the sites I and II.[56,57] According to the obtained results, it is concluded that the silver and zinc species were successfully exchanged with the CBV-600 zeolite and located inside the zeolite matrix.

3.4. Dynamic Light Scattering. Dynamic light scattering (DLS) makes possible to determine the hydrodynamic radius of nanoparticles. In the case of nanoparticles that have a spherical morphology, this parameter allows us to estimate the particle size quickly and without additional preparation. The hydrodynamic diameters of BMV and CCMV were determined using the DLS technique. The obtained data demonstrated the average diameter of 28.2 nm for both BMV and CCMV viruses (Figure 3), a characteristic for these species.[58] The hydrodynamic size shows how the particle behaves in a fluid. The mean particle size measured by DLS is highly sensitive to minor admixtures of particles larger than the size of the main fraction, such as aggregates, tenuous impurities in preparations, and dust.[59]

3.5. TEM Analysis. Figure 4 demonstrates the images obtained by TEM for the BMV, CCMV, and MS2 viruses. The particles diameter observed in TEM micrographs coincided well with that obtained using the DLS technique (see Figure 3). The BMV and CCMV and MS2 viruses presented uniform

https://doi.org/10.1021/acsomega.3c06462
ACS Omega 2024, 9, 7554−7563

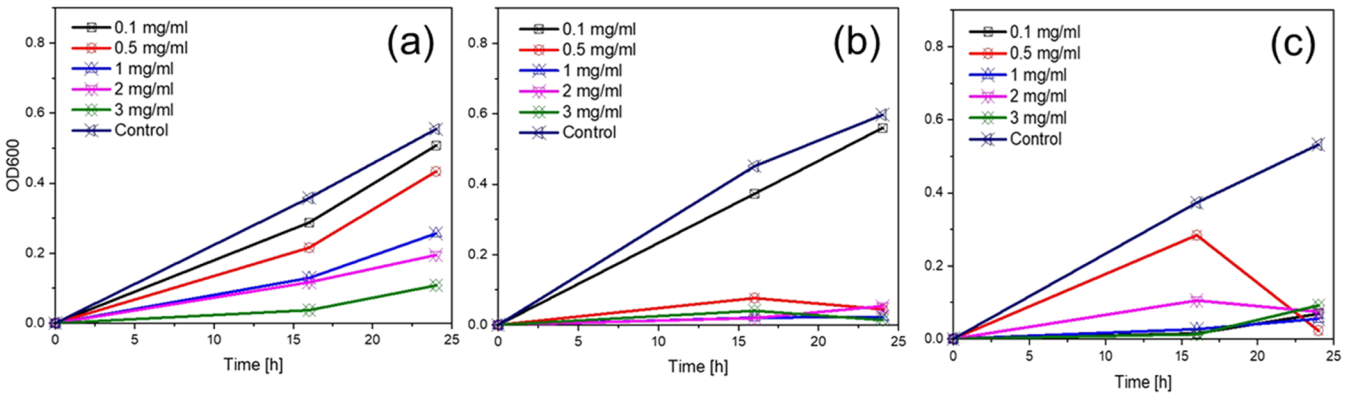

Figure 6. Antimicrobial activity of studied materials against *Staphylococcus aureus* in terms of optical density at 16 and 24 h: (a) Y-zeolite, (b) Ag/CBV-600, and (c) Zn/CBV-600.

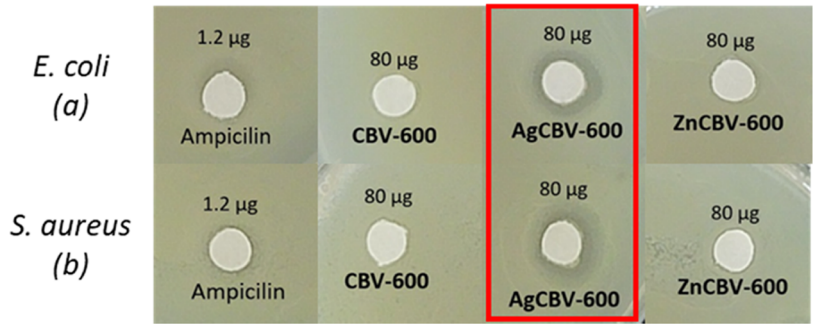

Figure 7. Bacterial susceptibility tests against (a) *E. coli* and (b) *S. aureus* for CBV-600, Ag/CBV-600, and Zn/CBV-600 samples.

monodisperse, well-defined particles with spherical morphology. However, particles for MS2 virus were not well organized compared to BMV and CCMV.

3.6. Antimicrobial Activity. The antimicrobial capacity of silver and zinc exchanged into Y-zeolite and their inhibition capacity at room temperature are presented in Figures 5 and 6. Figures show the growth of *E. coli* and *S. aureus* organisms in the absence and presence of nanomaterials. The control experiment shown in the graphs corresponds to normal growth of the bacteria without nanomaterials. Note that the Y-zeolite itself was characterized by an antibacterial activity against *E. coli* and *S. aureus* (Figures 5(a) and 6(a), respectively) similar to the data reported in refs 36,38. The growth inhibition of both microorganisms increased when the concentration of zeolite raised. Nevertheless, not all zeolite types demonstrate the bactericidal effect. As it was reported in ref 37, X-type zeolite did not exhibit any antimicrobial effect against *E. coli*, *S. aureus*, and *Pseudomonas aeruginosa*, yeast *Candida albicans*, and fungus *Aspergillus niger*. However, zeolite samples loaded with Zn^{2+} and Cu^{2+} showed excellent antimicrobial activity.[37] Faujasite exchanged with silver was chosen in ref 36 because it showed the highest biocidal action against *E. coli* among the studied samples exchanged with silver such as MCM-56 and ZSM-5.

The inhibitory function against *E. coli* and *S. aureus* increased when Ag^+ ions were present in the zeolite that is in the accordance with the literature data.[36,37,60] The concentration of the Ag/CBV-600 material influenced the bacterium inhibition rate for both *E. coli* and *S. aureus* (Figures 5(b) and 6(b), respectively). The strong effect of Ag^+ on the inhibition rate was observed starting at a relatively low concentration of the nanomaterial (0.5 mg/mL). The effect of silver ion concentration was reported in ref[38]. The authors mentioned that the higher the silver concentration, the greater the inhibition capacity of materials. However, in the present work, the inhibition capacity toward *E. coli* and *S. aureus* was obtained at low concentration (0.5 mg/mL) and a further increase of the nanomaterial concentration in LB medium did not affect the inhibition rate.

The Zn/CBV-600 nanomaterial demonstrated a fast-acting antibacterial effect at 16 h for concentrations ≥1 mg/mL. However, some growth of bacteria was observed at 24 h (Figures 5(c) and 6(c)). Those changes in the inhibitory capacity of the Zn/CBV-600 material for both *E. coli* and *S. aureus* bacteria may be attributed to the sedimentation of the nanomaterial in LB medium after 16 h of evaluation that may be a consequence of its hydrophobicity. A similar effect of decrease in the antimicrobial activity of the zeolite ion exchanged with Ag^+, Zn^{2+}, and Cu^{2+} ions toward *E. coli*. was observed in ref 61. Moreover, it was mentioned that the silver ions in zeolite have superior antimicrobial capacity compared to that of copper or zinc ions ($Ag^+ > Zn^{2+} > Cu^{2+}$). Ag/CBV-600 and Zn/CBV-600 nanomaterials prepared in the present work were characterized with higher antimicrobial efficacy against gram-negative bacteria *E. coli* at a similar concentration of nanomaterials (0.5−2 mg/mL) in comparison with analogous monometallic materials prepared on CBV-100 in ref 38.

There are some studies on the biocide capacity of metal ions that proposed the mechanism of their inhibitory effect: (i) direct contact of NPs with cell walls that leads to the destruction of bacterial cell integrity;[62,63] (ii) the production of reactive oxygen species (ROSs),[64−66] and (iii) the release of ions such as Ag^+ or Zn^{2+}.[8,14,67] The first two mechanisms are

https://doi.org/10.1021/acsomega.3c06462
ACS Omega 2024, 9, 7554−7563

Table 2. Adsorption Capacity of Brome Mosaic Virus (BMV), Cowpea Chlorotic Mottle Virus (CCMV), and Bacteriophage MS2 on Nanomaterials at 30, 60, and 120 min of Interaction

	adsorption capacity of virus with time, %								
	BMV			CCMV			MS2		
sample	30 min	60 min	120 min	30 min	60 min	120 min	30 min	60 min	120 min
CBV-600	11.7 ± 3.4	6.4 ± 4.1	4.5 ± 2.7	1.2 ± 0.7	6.9 ± 4.6	2.2 ± 1.2	11.4 ± 0.7	11.4 ± 0.7	11.5 ± 0.2
Ag/CBV-600	25.6 ± 2.4	24.2 ± 4.1	25.6 ± 1.5	39.2 ± 1.7	44.2 ± 1.2	43.5 ± 0.7	20.6 ± 0.4	20.6 ± 0.4	20.7 ± 1
Zn/CBV-600	23.8 ± 1.8	33.7 ± 4.0	31.3 ± 5.4	1.35 ± 0.6	7.3 ± 0.8	10.2 ± 4.3	21.3 ± 5	21.3 ± 5	31.2 ± 7.2

driven by the presence of NPs, either silver or zinc. ROSs include superoxide anions (O_2^-), hydroxyl radicals (HO_2^-), and hydrogen peroxide (H_2O_2), which can cause the destruction of cellular components such as DNA, proteins, and lipids.[64,65]

Another mechanism that affects the bacteria is the release of Ag^+ or Zn^{2+} ions. In this case, the positive charge of metal species is fundamental to have antimicrobial activity. When the released Ag^+ or Zn^{2+} adheres to the cytoplasmic membrane, proteins, and lipids due to the electrostatic attraction and affinity with sulfur proteins, this affects the permeability and mechanical properties of the bacteria. Ions located in the cytoplasm denature ribosomes and inhibit protein synthesis. In addition, ions affect the respiration process of the bacteria, causing a disruption of the membrane by reactive oxygen species.[68−70] As a result, the DNA molecules condense and lose their ability to replicate. Unusually, Ag^+ exhibits specific interactions with DNA, binding exclusively to natural bases instead of the negatively charged phosphate backbone.[71] Therefore, silver- or zinc-loaded zeolites studied in the present work are characterized by uniform distribution of cations in the zeolite structure that increases the ability to release the Ag^+ or Zn^{2+} ions during a long period of time. Thus, the zeolite serves as a useful carrier of silver or zinc ions with strong antibacterial activity.

Figure 7 shows the bacterial susceptibility tests against *E. coli* and *S. aureus* for CBV-600, Ag/CBV-600, and Zn/CBV-600 nanomaterials. After addition of 4 μL of stock solution with a concentration of 20 mg/mL, it was determined that there was approximately 80 μg of nanomaterial in each disk. The control ampicillin sample had an inhibition diameter of 0.93 cm. The bacterial susceptibility tests showed that the Ag/CBV-600 sample presented a well-defined inhibition halo both for *E. coli* and *S. aureus* (Figure 7(a,b) marked with red). The inhibition diameter obtained for Ag/CBV-600 was 1.06 cm. For the rest of the materials, the inhibition halo was barely perceptible. The latter may be explained by a diffusion phenomenon in the medium.[72]

The adsorption capacity of the studied nanomaterials with time was evaluated for BMV, CCMV, and MS2 viruses. The data are presented in Table 2. The reference CBV-600 zeolite sample was characterized by the relatively low ability to trap BMV and CCMV decreasing with the contact time of CBV-600 with viruses. In contrast, the opposite effect was observed for bacteriophage MS2. The adsorption capacity of MS2 was constant, reaching 11.5% at 30 min, and did not change with time. As it was mentioned above, some types of zeolites are characterized by antimicrobial properties *per se*,[30,31] especially faujasite mineral.[35,37] It may be assumed that the MS2 bacteriophage was characterized by lower resistance to CBV-600 than to BMV and CCMV. The adsorption capacity increased for CBV-600 modified with silver and zinc cations in comparison with pure CBV-600 (see Table 2). Both Ag/CBV-600 and Zn/CBV-600 were characterized with good adsorption capacity for BMV, CCMV, and MS2 viruses, reaching almost 45% after 120 min interaction time. However, some fluctuation of adsorption capacity was observed depending on the nature of the virus. For example, the maximum MS2 virus adsorption was obtained for Ag/CBV-600 at 30 min (ca. 21%) remaining constant during the rest of the experiment. However, the ability to trap the BMV and CCMV was higher for this sample (25 and 44%, respectively). The Zn/CBV-600 nanomaterial demonstrated good adsorption capacity for BMV and MS2 viruses getting almost 33% after 120 min interaction time. However, the opposite tendency was observed for CCMV, leading to the slight degradation of adsorption capacity (max 10% at 120 min). It can suppose that this behavior of the Zn/CBV-600 material may be related to the fact that such a heavy metal as zinc is not an essential element for the CCMV. For example, there are few cases where some pathogens were found resistant to Cu ions.[73] On the other hand, some drop of adsorption capacity may be caused by the reduction of silver and zinc cations with formation of NPs in LB medium and its agglomeration and, as a consequence, the decrease in the adsorption capacity of the studied nanomaterials. It is well known that the large size of particles reduces its dispersibility and efficiency, weakening the antimicrobial activity of the material. A similar effect was reported in ref 60 for Ag/TiO_2 NPs.

The antimicrobial activity of zeolite-based nanomaterials showed that the methodology used for the preparation of the materials and the tested microorganisms is a very important factor and demands careful selection of parameters to achieve better antimicrobial performance.

4. CONCLUSIONS

The aim of the present research is to find an alternative to antimicrobial materials based on nanoparticles that would contain active silver and zinc immobilized into a solid matrix that prevents their agglomeration and migration to the environment. For this purpose, silver and zinc ions were successfully exchanged with hydrogen cations of Y-zeolite in a proportion of 1 atomic %. The ion exchange procedure does not modify the Y-zeolite structure. According to the result obtained using the UV−visible technique, the dominant species in the zeolite are Ag^+ and Zn^{2+} cations. The antimicrobial test against strains of bacteria *Escherichia coli* and *Staphylococcus aureus* on the Ag/CBV-600 and Zn/CBV-600 nanomaterials demonstrates high inactivation capacity for both bacteria, starting at a relatively low concentration of nanomaterial (0.5 mg). Moreover, the samples present good adsorption capacity for plant BMV and CCMV; both Ag/CBV-600 and Zn/CBV-600 show CCMV adsorption percentages higher than 40% after 2 h of interaction with the virus. The silver or zinc cations, uniformly distributed in the zeolite

https://doi.org/10.1021/acsomega.3c06462
ACS Omega 2024, 9, 7554−7563

structure, increased the ability to release the Ag^+ or Zn^+ cations during a long period of time and serve as a useful carrier with a strong antibacterial activity. Therefore, it is expected that the materials synthesized in the present work become a long-lasting antimicrobial agent. The obtained results allow further investigation of presently prepared nanomaterials as an effective remedy to inhibit and reduce the spread of viruses such as SARS-CoV-2 or other gram-positive or gram-negative bacteria. The prepared nanomaterials may be used for fabric functionalization applied for confection of personal and medical protection utensils.

AUTHOR INFORMATION

Corresponding Author

Elena Smolentseva − *Universidad Nacional Autónoma de México, Centro de Nanociencias y Nanotecnología, C.P. 22860 Ensenada, Baja California, México;* orcid.org/0000-0003-2562-9094; Email: elena@ens.cnyn.unam.mx

Authors

Perla Sánchez-López − *Universidad Nacional Autónoma de México, Centro de Nanociencias y Nanotecnología, C.P. 22860 Ensenada, Baja California, México*

Kevin A. Hernández-Hernández − *Universidad Nacional Autónoma de México, Centro de Nanociencias y Nanotecnología, C.P. 22860 Ensenada, Baja California, México; Centro de Investigación Científica y de Educación Superior de Ensenada (CICESE), C.P. 22860 Ensenada, Baja California, México*

Sergio Fuentes Moyado − *Universidad Nacional Autónoma de México, Centro de Nanociencias y Nanotecnología, C.P. 22860 Ensenada, Baja California, México*

Rubén D. Cadena Nava − *Universidad Nacional Autónoma de México, Centro de Nanociencias y Nanotecnología, C.P. 22860 Ensenada, Baja California, México*

Complete contact information is available at: https://pubs.acs.org/10.1021/acsomega.3c06462

Notes

The authors declare no competing financial interest.

ACKNOWLEDGMENTS

The authors thank Dr. Rosario Isidro Yocupicio and M.C. Fabian Humberto Alonso for their technical support. This work was supported by DGAPA-PAPIIT (UNAM, México) through the project IV-100121. P.S.-L. thanks CONAHCYT for the grant "Estancias posdoctorales por México".

REFERENCES

(1) Patil, M. P.; Kim, G.-D. Eco-friendly approach for nanoparticles synthesis and mechanism behind antibacterial activity of silver and anticancer activity of gold nanoparticles. *Appl. Microbiol. Biotechnol.* **2017**, *101* (1), 79−92.

(2) Sarkar, J.; Achary, K. Alternaria alternata culture filtrate mediated bioreduction of chloroplatinate to platinum nanoparticles. *Inorganic Nano-met. Chem.* **2017**, *47*, 365−369.

(3) Kästner, C.; Thü, A. F. Catalytic Reduction of 4-Nitrophenol using silver nanoparticles with adjustable activity. *Langmuir* **2016**, *32* (29), 7383−7391.

(4) Elegbede, J. A.; Lateef, A. Green synthesis of silver (Ag), gold (Au) and silver-gold (Ag-Au) alloy nanoparticles: a review on recent advances, trends and biomedical applications. In *Nanotechnology and Nanomaterial Applications in Food, Health and Biomedical Sciences*; Verma, D. K.; Goyal, M. R.; Suleria, H. A. R., Eds.; Apple Academic Press Inc, CRC Press, Taylor and Francis Group: Oakville, Ontario, Canada, 2019; pp 3−89.

(5) Lateef, A.; Elegbede, J. A.; Akinola, P. O.; Ajayi, V. A. Biomedical applications of green synthesized-metallic nanoparticles: a review. *Pan Afr. J. Life Sci.* **2019**, *3*, 157−182.

(6) Sahoo, S. K.; Parveen, S.; Panda, J. J. The present and future of nanotechnology in human health care. *Nanomedicine* **2007**, *3* (1), 20−31.

(7) Kim, J. S.; Kuk, E.; Yu, K. N.; Kim, J. H.; Park, S. J.; Lee, H. J.; Kim, S. H.; Park, Y. K.; Park, Y. H.; Hwang, C. Y.; Kim, Y. K.; Lee, Y. S.; Jeong, D. H.; Cho, M. H. Antimicrobial effects of silver nanoparticles. *Nanomedicine* **2007**, *3* (1), 95−101.

(8) Yin, I. X.; Zhang, J.; Zhao, S. I.; Mei, M. L.; Li, Q.; Chu, C. H. The antibacterial mechanism of silver nanoparticles and its application in dentistry. *Int. J. Nanomed.* **2020**, *15*, 2555−2562.

(9) Kim, J. S.; Kuk, E.; Yu, K. N.; Kim, J.-H.; Park, S. J.; Lee, H. J.; Kim, S. H.; Park, Y. K.; Park, Y. H.; Hwang, C.-Y.; Kim, Y.-K.; Lee, Y.-S.; Jeong, D. H.; Cho, M.-H. Antimicrobial effects of silver nanoparticles. *Nanomedicine* **2007**, *3* (1), 95−101.

(10) Maiti, S.; Krishnan, D.; Barman, G.; Barman, G.; Ghosh, S. K.; Laha, J. K. Antimicrobial activities of silver nanoparticles synthesized from Lycopersicon esculentum extract. *J. Anal. Sci. Technol.* **2014**, *5* (40), 1−7, DOI: 10.1186/s40543-014-0040-3.

(11) Pietrzak, K.; Gutarowska, B.; Machnowski, W.; Mikołajczyk, U. Antimicrobial properties of silver nanoparticles misting on cotton fabrics. *Text. Res. J.* **2016**, *86* (8), 812−822.

(12) Kalwar, K.; Shan, D. Antimicrobial effect of silver nanoparticles (AgNPs) and their mechanism − a mini review. *Micro Nano Lett.* **2018**, *13* (3), 277−280.

(13) Bruna, T.; Maldonado-Bravo, F.; Jara, P.; Caro, N. Silver nanoparticles and their antibacterial applications. *Int. J. Molecular Sci.* **2021**, *22* (13), 7202.

(14) Khorrami, S.; Zarrabi, A.; Khaleghi, M.; Danaei, M.; Mozafari, M. R. Selective cytotoxicity of green synthesized silver nanoparticles against the MCF-7 tumor cell line and their enhanced antioxidant and antimicrobial properties. *Inter. J. Nanomed.* **2018**, *Volume 13*, 8013−8024.

(15) Urnukhsaikhan, E.; Bold, B. E.; Gunbileg, A.; Sukhbaatar, N.; Mishig-Ochir, T. Antibacterial activity and characteristics of silver nanoparticles biosynthesized from Carduus crispus. *Sci. Rep.* **2021**, *11*, No. 21047.

(16) Loo, Y. Y.; Rukayadi, Y.; Nor-Khaizura, M.-A.-R.; Kuan, C. H.; Chieng, B. W.; Nishibuchi, M.; Radu, S. In Vitro Antimicrobial activity of green synthesized silver nanoparticles against selected gram-negative foodborne pathogens. *Front. Microbiol.* **2018**, *9*, 1555.

(17) Firouzabadi, F. B.; Noori, M.; Edalatpanah, N. M.; Edalatpanah, Y.; Mirhosseini, M. ZnO nanoparticle suspensions containing citric acid as antimicrobial to control Listeria monocytogenes, *Escherichia coli*, *Staphylococcus aureus* and Bacillus cereus in mango juice. *Food Control.* **2014**, *42*, 310−314.

(18) Rai, M. Nanobiotecnologia verde: biossínteses de nano-particulas metálicas e suas aplicações como nanoantimicrobianos. *Cienc. Cult.* **2013**, *65* (3), 44−48.

(19) Raghupathi, K. R.; Koodali, R. T.; Manna, A. C. Size-dependent bacterial growth inhibition and mechanism of antibacterial activity of zinc oxide nanoparticles. *Langmuir* **2011**, *27* (7), 4020−4028.

(20) Manoharan, C.; Pavithra, G.; Dhanapandian, S.; Dhamodaran, P.; Shanthi, B. Properties of spray pyrolised ZnO: Sn thin films and their antibacterial activity. *Spectrochim Acta Part A* **2015**, *141*, 292−299.

(21) Janaki, A. C.; Sailatha, E.; Gunasekaran, S. Synthesis, characteristics and antimicrobial activity of ZnO nanoparticles. *Spectrochim Acta Part A* **2015**, *144*, 17−22.

(22) Sirelkhatim, A.; Mahmud, S.; Seeni, A.; Kaus, N. H. M.; Ann, L. C.; Bakhori, S. K. M.; Hasan, H.; Mohamad, D. Review on zinc oxide nanoparticles: antibacterial activity and toxicity mechanism. *Nano-Micro Lett.* **2015**, *7* (3), 219−242.

(23) Gupta, V. K.; Atar, N.; Yola, M. L.; Üstündağ, Z.; Uzun, L. A novel magnetic Fe@Au core-shell nanoparticles anchored graphene

oxide recyclable nanocatalyst for the reduction of nitrophenol compounds. *Water Res.* **2014**, *48*, 210−217.
(24) Hoseini, S. J.; Bahrami, M.; Sadri, N.; Aramesh, N.; Fard, Z. S.; Iran, H. R.; Agahi, B. H.; Maddahfar, M.; Dehghani, M.; Arabi, A. Z. B.; Heidari, N.; Fard, S. F. H.; Moradi, Z. Multi-metal nanomaterials obtained from oil/water interface as effective catalysts in reduction of 4-nitrophenol. *J. Colloid Interface Sci.* **2018**, *513*, 602−616.
(25) El-Bahy, Z. M.; Hanafy, A. I.; El-Bahy, S. M. Preparation of Pt, Pd and Cu nano single and bimetallic systems-supported NaY zeolite and test their activity in p-nitrophenol reduction and as anticancer agents. *J. Environ. Chem. Eng.* **2019**, *7*, No. 103117.
(26) Goyal, A.; Bansal, S.; Kumar, V.; Singh, J.; Singhal, S. Mn substituted cobalt ferrites (CoMnxFe2−xO4 (x = 0.0, 0.2, 0.4, 0.6, 0.8, 1.0)): As magnetically separable heterogeneous nanocatalyst for the reduction of nitrophenols. *Appl. Surf. Sci.* **2015**, *324*, 877−889.
(27) Shi, X.; Quan, S.; Yang, L.; Shi, G.; Shi, F. Facile synthesis of magnetic Co3O4/BFO nanocomposite for effective reduction of nitrophenol isomers. *Chemosphere.* **2019**, *219*, 914−922.
(28) Inoue, Y.; Hoshino, M.; Takahashi, H.; Noguchi, T.; Murata, T.; Kanzaki, Y.; Hamashima, H.; Sasatsu, M. Bactericidal Activity of Ag-zeolite mediated by reactive oxygen species under aerated conditions. *Journal of Inorganic Biochemistry* **2002**, *92*, 37−42.
(29) Demirci, S.; Ustaoğlu, Z.; Yılmazer, G. A.; Sahin, F.; Baç, N. Antimicrobial properties of zeolite-X and zeolite-A ion-exchanged with silver, copper, and zinc against a broad range of microorganisms. *Appl. Biochem. Biotechnol.* **2014**, *172*, 1652.
(30) Hrenovic, J.; Milenkovic, J.; Ivankovic, T.; Rajic, N. Antibacterial activity of heavy metal-loaded natural zeolite. *J. Hazard. Mater.* **2012**, *201*−*202*, 260−264.
(31) Ferreira, L.; Guedes, J. F.; Almeida-Aguiar, C.; Fonseca, A. M.; Neves, I. C. Colloids essential oils encapsulated in zeolite structures as delivery systems (EODS): An overview. *Molecules* **2016**, *142*, 141−147.
(32) Dikić, J.; Lukić, I.; Pajnik, J.; Pavlović, J.; Hrenović, J.; Rajić, N. Antibacterial activity of thymol/carvacrol and clinoptilolite composites prepared by supercritical solvent impregnation. *J. Porous Mater.* **2021**, *28*, 1577.
(33) Jaime-Acuña, O. E.; Meza-Villezcas, A.; Vasquez-Peña, M.; Raymond-Herrera, O.; Villavicencio-García, H.; Petranovskii, V.; Vazquez-Duhalt, R.; Huerta-Saquero, A. Synthesis and Complete Antimicrobial Characterization of CEOBACTER, an Ag-Based Nanocomposite. *PLoS One* **2016**, *11* (11), No. e0166205.
(34) Zhang, Y.; Zhong, S.; Zhang, M.; Lin, Y. Antibacterial activity of silver-loaded zeolite A prepared by a fast microwave-loading method. *J. Mater. Sci.* **2009**, *44*, 457−462.
(35) Kwakye-Awuah, B.; Williams, C.; Kenward, M.; Radecka, I. Antimicrobial action and efficiency of silver-loaded zeolite X. *J. Appl. Microbiol.* **2008**, *104*, 1516−1524.
(36) Jędrzejczyk, R. J.; Turnau, K.; Jodłowski, P. J.; Chlebda, D. K.; Łojewski, T.; Łojewska, J. Antimicrobial properties of silver cations substituted to faujasite mineral. *J. Nanomaterials* **2017**, *7* (9), 240.
(37) Tekin, R.; Bac, N. Antimicrobial behavior of ion-exchanged zeolite X containing fragrance. *Microporous Mesoporous Mater.* **2016**, *234* (1), 55−60.
(38) Ferreira, L.; Almeida-Aguiar, C.; Parpot, P.; Fonseca, A. M.; Neves, I. C. Preparation and assessment of antimicrobial properties of bimetallic materials based on NaY zeolite. *RSC Adv.* **2015**, *5*, 37188−37195.
(39) Sánchez-López, P.; Kotolevich, Y.; Miridonov, S.; Chávez-Rivas, F.; Fuentes, S.; Petranovskii, V. Bimetallic AgFe systems on mordenite: effect of cation deposition order in the NO reduction with C_3H_6/CO. *Catalysts.* **2019**, *9*, 58.
(40) Cadena-Nava, R. D.; Comas-Garcia, M.; Garmann, R. F.; Rao, A. L. N.; Knobler, C. M.; Gelbart, W. M. Self-assembly of viral capsid protein and RNA molecules of different sizes: requirement for a specific high protein/RNA mass ratio. *J. Virol.* **2012**, *86* (6), 3318−3326.
(41) Sánchez-López, P.; Antúnez-García, J.; Fuentes-Moyado, S.; Galván, D. H.; Petranovskii, V.; Chávez-Rivas, F. Analysis of theoretical and experimental X-ray diffraction patterns for distinct mordenite frameworks. *J. Mater. Sci.* **2019**, *54*, 7745−7757.
(42) Li, S.; Cai, K.; Li, Y.; Liu, S.; Yu, M.; Wang, Y.; Ma, X.; Huang, S. Identifying the active silver species in carbonylation of dimethyl ether over Ag-HMOR. *ChemCatChem* **2020**, *12*, 3290.
(43) Ul'yanova, N. Yu.; Golubeva, O. Yu. Zeolites modified with silver nanoparticles and clusters: synthesis, characterization, and catalytic performance in H2 and CO oxidation reactions. *Glass Phys. Chem.* **2018**, *44* (5), 418−422.
(44) Dong, B.; Retoux, R.; de Waele, V.; Chiodo, S. G.; Mineva, T.; Cardin, J.; Mintova, S. Sodalite cages of EMT zeolite confined neutral molecular-like silver clusters. *Microporous Mesoporous Mater.* **2017**, *244*, 74−82.
(45) Horta Fraijo, P.; Smolentseva, E.; Simakov, A.; José-Yacaman, M.; Acosta, B. Ag nanoparticles in A4 zeolite as efficient catalysts for the 4-nitrophenol reduction. *Microporous Mesoporous Mater.* **2021**, *312*, No. 110707.
(46) Torres-Flores, E. I.; Flores-López, N. S.; Martínez-Núñez, C. E.; Tánori-Córdova, J. C.; Flores-Acosta, M.; Cortez-Valadez, M. Silver nanoparticles in natural zeolites incorporated into commercial coating: antibacterial study. *Appl. Phys. A: Mater. Sci. Process.* **2021**, *127* (1), 1−11, DOI: 10.1007/s00339-020-04227-5.
(47) Azambre, B.; Chebbi, M.; Hijazi, A. Effects of the cation and Si/Al ratio on CH3I adsorption by faujasite zeolites. *Chem. Eng. J.* **2020**, *379*, No. 122308.
(48) Martinez-Ortigosa, J.; Lopes, C. W.; Agostini, G.; Palomares, A. E.; Blasco, T.; Rey, F. AgY zeolite as catalyst for the selective catalytic oxidation of NH3. *Microporous Mesoporous Mater.* **2021**, *323*, No. 111230.
(49) Aparicio-Vázquez, S.; Fall, C.; Islas-Espinoza, M.; Alcántara, D.; Petranovskii, V.; Olguín, M. T. Influence of experimental conditions to obtain silver-modified zeolite-rich tuffs on the antimicrobial activity for *Escherichia coli* suspended in aqueous media. *Environ. Technol. Innovation* **2021**, *23*, No. 101707.
(50) Kolobova, E.; Pestryakov, A.; Mamontov, G.; Kotolevich, Y.; Bogdanchikova, N.; Farias, M.; Vosmerikov, A.; Vosmerikova, L.; Cortes Corberan, V. Low-temperature CO oxidation on Ag/ZSM-5 catalysts: Influence of Si/Al ratio and redox pretreatments on formation of silver active sites. *Fuel* **2017**, *188*, 121−131.
(51) Yamamoto, T.; Takenaka, S.; Tanaka, T.; Baba, T. Stability of silver cluster in zeolite A and Y catalysts. *J. Phys.: Conf. Ser.* **2009**, *190*, No. 012171.
(52) Shimizu, K.-i.; Sugino, K.; Kato, K.; Yokota, S.; Okumura, K.; Satsuma, A. Formation and Redispersion of Silver Clusters in Ag-MFI Zeolite as Investigated by Time-Resolved QXAFS and UV−Vis. *J. Phys. Chem. C* **2007**, *111* (4), 1683−1688.
(53) Mintcheva, N.; Panayotova, M.; Gicheva, G.; Gemishev, O.; Tyuliev, G. Effect of exchangeable ions in natural and modified zeolites on Ag content, Ag nanoparticle formation and their antibacterial activity. *Materials* **2021**, *14* (15), 4153.
(54) Alswat, A. A.; Ahmad, M. B.; Saleh, T. A.; Hussein, M. Z. B.; Ibrahim, N. A. Effect of zinc oxide amounts on the properties and antibacterial activities of zeolite/zinc oxide nanocomposite. *Mater. Sci. Eng.: C* **2016**, *68*, 505−511.
(55) Chen, J.; Feng, Z.; Ying, P.; Li, C. ZnO clusters encapsulated inside micropores of zeolites studied by UV Raman and Laser-Induced Luminescence spectroscopies. *J. Phys. Chem. B* **2004**, *108* (34), 12669−12676.
(56) Seo, S. M.; Lim, W. T.; Seff, K. Crystallographic verification that copper (II) coordinates to four of the oxygen atoms of zeolite 6-rings. two single-crystal structures of fully dehydrated, largely Cu^{2+}-exchanged zeolite y (FAU, Si/Al = 1.56). *J. Phys. Chem. C* **2012**, *116*, 963−974.
(57) Lee, Y. M.; Choi, S. J.; Kim, Y.; Seff, K. Crystal structure of an ethylene sorption complex of fully vacuum-dehydrated fully Ag^{+}-exchanged zeolite X (FAU). Silver atoms have reduced ethylene to give CH_2^{2-} carbanions at framework oxide vacancies. *J. Phys. Chem. B* **2005**, *109* (43), 20137−20144.

https://doi.org/10.1021/acsomega.3c06462
ACS Omega 2024, 9, 7554−7563

(58) Bockstahler, L. E.; Kaesberg, P. The molecular weight and other biophysical properties of bromegrass mosaic virus. *Biophys. J.* **1962**, *2* (1), 1−9.
(59) Nikitin, N.; Trifonova, E.; Evtushenko, E.; Kirpichnikov, M.; Atabekov, J.; Karpova, O. Comparative study of non-enveloped icosahedral viruses size. *PLoS One* **2015**, *10* (11), No. e0142415.
(60) Bao, S.; Sun, S.; Li, L.; Xu, L. Synthesis and antibacterial activities of Ag-TiO_2/ZIF-8. Front. *Bioeng. Biotechnol.* **2023**, *11*, No. 1221458.
(61) Demirci, S.; Ustaoğlu, Z.; Yılmazer, G. A.; Sahin, F.; Baç, N. Antimicrobial properties of zeolite-X and zeolite-A ion-exchanged with silver, copper, and zinc against a broad range of microorganisms. *Appl. Biochem. Biotechnol.* **2014**, *172* (3), 1652−1662.
(62) Brayner, R.; Ferrari-Iliou, R.; Brivois, N.; Djediat, S.; Benedetti, M. F.; Fiévet, F. Toxicological impact studies based on *Escherichia coli* bacteria in ultrafine ZnO nanoparticles colloidal medium. *Nano Lett.* **2006**, *6* (4), 866−870.
(63) Zhang, L.; Jiang, Y.; Ding, Y.; Povey, M.; York, D. Investigation into the antibacterial behaviour of suspensions of ZnO nanoparticles (ZnO nanofluids). *J. Nanopart. Res.* **2007**, *9* (3), 479−489.
(64) Kiwi, J.; Nadtochenko, V. Evidence for the mechanism of photocatalytic degradation of the bacterial wall membrane at the TiO_2 interface by ATR-FTIR and laser kinetic spectroscopy. *Langmuir* **2005**, *21* (10), 4631−4641.
(65) Padmavathy, N.; Vijayaraghavan, R. Enhanced bioactivity of ZnO nanoparticles - an antimicrobial study. *Sci. Technol. Adv. Mater.* **2008**, *9*, No. 035004.
(66) Raghupathi, K. R.; Koodali, R. T.; Manna, A. C. Size-dependent bacterial growth inhibition and mechanism of antibacterial activity of zinc oxide nanoparticles. *Langmuir* **2011**, *27* (7), 4020−4028.
(67) Kadiyala, U.; Turali-Emre, E. S.; Bahng, J. H.; Kotov, N. A.; Van Epps, J. S. Unexpected insights into antibacterial activity of zinc oxide nanoparticles against methicillin resistant *Staphylococcus aureus* (MRSA). *Nanoscale* **2018**, *10* (10), 4927−4939.
(68) Yin, I. X.; Zhang, J.; Zhao, I. S.; Mei, M. L.; Li, Q.; Chu, C. H. The Antibacterial mechanism of silver nanoparticles and its application in dentistry. *Int. J. Nanomed.* **2020**, *15*, 2555−2562.
(69) Landini, P.; Antoniani, D.; Burgess, J. G.; Nijland, R. Molecular mechanisms of compounds affecting bacterial biofilm formation and dispersal. *Appl. Microbiol. Biotechnol.* **2010**, *86* (3), 813−823.
(70) Pasquet, J.; Chevalier, Y.; Couval, E.; Bouvier, D.; Bolzinger, M.-A. Zinc oxide as a new antimicrobial preservative of topical products: interactions with common formulation ingredients. *Int. J. Pharm.* **2015**, *479* (1), 88−95.
(71) Swasey, S. M.; Leal, L. E.; Lopez-Acevedo, O.; Pavlovich, J.; Gwinn, E. G. Silver (I) as DNA glue: Ag^+-mediated guanine pairing revealed by removing Watson-Crick constraints. *Sci. Rep.* **2015**, *5* (1), No. 10163.
(72) Bauer, A. W.; Kirby, W. M.; Sherris, J. C.; Turck, M. Antibiotic susceptibility testing by a standardized single disk method. *Am. J. Clin. Pathol.* **1966**, *45* (4), 493−496.
(73) Ding, C.; Festa, R. A.; Chen, Y. L.; Espart, A.; Palacios, O.; Espln, J.; Capdevila, M.; Atrian, S.; Heitman, J.; Thiele, D. J. Cryptococcus neoformans copper detoxifcation machinery is critical for fungal virulence. *Cell Host Microbe.* **2013**, *13*, 265−276.

https://doi.org/10.1021/acsomega.3c06462
ACS Omega 2024, 9, 7554−7563